Long-term stable solid concentrated graphene dispersion assisted by a highly aromatic ionic liquid

Soha Aldroubi, Eric Anglaret, Ibrahim Bou Malham, Peter Hesemann, Nicolas Brun, Ahmad Mehdi

Long-term stable solid concentrated graphene dispersion assisted by a highly aromatic ionic liquid

Soha Aldroubi[a,b], Eric Anglaret[c], Ibrahim Bou Malham[b], Peter Hesemann[a], Nicolas Brun[a]* and Ahmad Mehdi[a]*

[a]*ICGM, Univ Montpellier, CNRS, ENSCM, Montpellier, France.*

[b]*Laboratoire Energétique et Réactivité à l'Echelle Nanométrique (EREN), Faculté des Sciences IV, Université Libanaise, Haouch el-Omara, 1801 Zahlé, Liban.*

[c]*L2C, Univ Montpellier, CNRS, Montpellier, France.*

*Corresponding authors: Pôle de recherche Balard – ICGM, Campus CNRS, 1919, route de Mende, 34293 Montpellier, FRANCE
E-mail addresses: nicolas.brun@enscm.fr; ahmad.mehdi@umontpellier.fr
Telephone numbers: +33 (0)4 48 79 20 98 (N. Brun); +33 (0)4 48 79 20 96 (A. Mehdi)

Elsevier use only: Received date here; revised date here; accepted date here

Abstract

Hypothesis. The sonochemical exfoliation of graphite in solution has been demonstrated as a promising and easy technique for producing graphene dispersions. This is usually done in organic solvents and leads to unstable dispersions with very low graphene concentration. Ionic liquids (ILs) represent a versatile and safe alternative to traditional organic solvents. A few recent studies reported the use of commercial ILs with bulky anions, such as bis(trifluoromethylsulfonyl)imide, and aromatic cations, such as imidazolium, which favour the exfoliation of graphite through π-π and cation-π interactions. Although recently investigated, the role of aromatic groups on imidazolium cations is still controversial and systematic studies are still necessary. Besides, these studies were limited to liquid dispersions at room temperature. **Experiments.** Herein, we prepared four highly aromatic imidazolium-based ILs, including the newly reported 1-(naphthylmethyl)-3-benzylimidazolium bis(trifluoromethanesulfonyl)imide, [(Np)(Bn)im][NTf_2]. These ILs were used for the sonochemical exfoliation of graphite and compared with a commercial benchmark, 1-butyl-3-methylimidazolium bis(trifluoromethylsulfonyl)imide [Bmim][NTf_2]. **Findings.** Interestingly, [(Np)(Bn)im][NTf_2] allowed reaching solid dispersions at room temperature containing thin few layer graphene sheets with long-term stability (up to 2 years) and high concentration (3.6 mg/mL). Such graphene dispersion combines long-term stability in the solid-state and high processability in the liquid state, by a simple heating above 60 °C.

Keywords : *Ionic liquid, imidazolium, graphite exfoliation, sonochemical exfoliation, graphene, solid dispersion.*

1. Introduction

Ionic liquids (ILs) have been the focus of much attention because of their singular physicochemical properties together with a great applicative potential in different fields [1]. The term "ionic liquid" designates any salt having a melting point below the boiling point of water [2]. ILs generally consist of an organic cation and an inorganic anion [3]. The large variety of possible anion-cation combinations provides a fine adjustment of their physicochemical properties. Many ILs, but not all, are non-flammable, relatively non-toxic (even though some ILs are even more toxic to microorganisms than traditional solvents [4]), non-volatile and display high calorific capacity and high thermal stability. Even though ILs are not intrinsically greener than traditional solvents, they can contribute to make chemical processes greener [5]. Thus, the use of wisely selected ILs can make chemical processes meet most of the requirements of the green chemistry principles [6]. For instance, due to their unique physicochemical properties, ILs can promote the exfoliation of two-dimensional materials and more specifically graphite [7-15]. Some ILs, such as imidazolium-based ILs, exhibit a surface tension that closely matches the surface energy of graphite [16]. Consequently, they can favour the spontaneous exfoliation of graphite into discrete graphene sheets at room temperature. As reported by Atkin *et al.*, imidazolium cations can intercalate between two graphene sheets at the step edges of highly ordered pyrolytic graphite, thus weakening the energy barrier and favouring the intercalation of the next cations [17]. Strong cation-π electrostatic and π-π stacking interactions are two key factors for the stabilization and functionalization of graphene sheets, especially in imidazolium-based ILs [18-21].

The exfoliation of graphite into graphene can be favoured by sonochemistry in a liquid phase [22-24]. Then, the sonochemical exfoliation of graphite into mono, bi and few layers of graphene (FLG) is promoted by the collapse of cavitation bubbles in the liquid that can generate strong shear forces, which weaken the interlayer interaction [25, 26]. Sonochemistry is one of the most effective method for the exfoliation of graphite because it often yields stable and high quality graphene dispersions and the sp^2-hybridized network of the as-obtained graphene sheets can be preserved [27]. The liquid phase exfoliation of graphite was first reported in toxic organic solvents like NMP, DMF and DMSO which only lead to very low FLG concentrations, below 0.01 mg/mL [16, 21]. Recently, alternative solvents have been used such as water [28] and cyrene [29]. Besides, graphenide (*i.e.*, negatively charged graphene) solutions can be obtained from graphite intercalation compounds after exfoliation down to single layers in tetrahydrofuran (THF) [30-32]. In the work of Bepete *et al.*, homogeneous single layer graphene (SLG) dispersions were obtained by mixing graphenide solutions with degassed water. After evaporating THF, SLG long-term stable aqueous dispersions with a concentration of 0.16 mg/mL were obtained [28]. In another recent example, cyrene, a biosourced solvent, was used to exfoliate graphite, yielding graphene dispersion with a relatively high concentration up to 0.24 mg/mL [29].

In this context, ILs offer a promising alternative for the exfoliation of graphite since they allowed achieving graphene dispersions with higher concentrations and long-term stability [33]. For instance, Wang *et al.* [15] used a commercial IL, *i.e.*, 1-butyl-3-methylimidazolium bis(trifluoromethylsulfonyl)imide [Bmim][NTf_2], for the sonochemical exfoliation of graphite (1 hour at 750 W). They obtained a few layer graphene (FLG) dispersion with a concentration of 0.95 mg/mL. More recently, Bari *et al.* [34] studied ILs containing imidazolium cations bearing aromatic benzyl side groups, *i.e.*, 1-benzyl-3-methylimidazolium and 1,3-bis(benzyl)imidazolium bis(trifluoromethanesulfonyl)imide, namely [(Bn)mim][NTf_2] and [$(Bn)_2$im][NTf_2], respectively. While an unstable dispersion was obtained with [Bmim][NTf_2], a stable one was obtained with [(Bn)mim][NTf_2], with a concentration of 0.081 mg/mL. Interestingly, [$(Bn)_2$im][NTf_2] yielded a liquid dispersion with a significantly higher concentration of graphene of 5.8 mg/mL, probably due to very strong π-π interactions favoured by the two benzyl side groups oriented nearly parallel to the graphene surface [34]. However, the role of aromatic groups on imidazolium cations is still controversial. Density-

functional theory (DFT) calculations performed by R.K Donato *et al.* [35] showed that the imidazolium ring in $[(Bn)_2im]^+$ cations has a more intimate binding with the surface of graphene sheets than the benzyl side groups. Besides, the effect of the anion was evidenced; small anions like bromide negatively affected the exfoliation while bulky anions such as bis(trifluoromethanesulfonyl)imide stabilized large exfoliated graphene sheets, as confirmed by Paduà *et al.* [36]. R.K Donato *et al.* [35] showed that aromatic anions, *i.e.*, benzoate and 1-naphtoate, associated to $[(Bn)_2im]^+$ cations presented more favorable binding energies with graphene than bis(trifluoromethanesulfonyl)imide. In most of these studies, imidazolium-based ILs bearing aromatic benzyl side groups provided FLG liquid dispersions (< 5 layers) with very little information about stability over time.

Furthermore, it was demonstrated that the addition of naphthalene promotes the exfoliation of graphite in organic solvents such as N-methyl-2-pyrrolidone, and allows achieving a graphene concentration higher than 0.15 mg/mL after only 90 min of sonication [37]. Hence, the functionalization of imidazolium cation with naphthyl groups appears as a good option to favour the exfoliation of graphite.

Herein, we report an original imidazolium bis(trifluoromethanesulfonyl)imide IL, which is solid at room temperature and bears both a benzyl and a naphthyl group on the cation. The exfoliation of natural graphite particles was carried out by sonochemistry in an ultrasonic bath. Interestingly, solid graphene dispersions containing thin few layer graphene sheets with long-term stability and high concentration (ca. 3.6 mg/mL) were obtained.

2. Experimental section

2.1. Materials

Imidazole (99 % purity), benzyl bromide (98 %), 2-(bromomethyl)naphthalene (96 %), lithium bis(trifluoromethanesulfonyl)imide (99 %), sodium hydride (60% in mineral oil), 1-methylimidazole (99 %) and graphite flakes (+100 mesh particle size, ≥75 % min) were purchased from Sigma Aldrich. [Bmim][NTf_2] (99.5 %) was purchased from IoLiTec. All the ILs reported herein were synthesized and purified in our laboratory, except for [Bmim][NTf_2] (**IL1**). The synthetic procedures and characterizations for [(Bn)mim][NTf_2] (**IL2**), 1-(naphthylmethyl)-3-methylimidazolium bis(trifluoromethanesulfonyl)imide, namely [(Np)mim][NTf_2] (**IL3**), and $[(Bn)_2im][NTf_2]$ (**IL4**) can be found in the supplementary information section (Fig. S4-S6). The synthetic procedure used to prepare 1-(naphthylmethyl)-3-benzylimidazolium bis(trifluoromethanesulfonyl)imide, namely [(Np)(Bn)im][NTf_2] (**IL5**), is described hereafter in section 2.2.

*2.2. Synthesis of [(Np)(Bn)im][NTf_2] (**IL5**)*

In a typical procedure (Scheme 1), imidazole (5.31 g, 78 mmol) was mixed with an equimolar amount of sodium hydride (3.12 g (60 % dispersion in mineral oil), 78 mmol) in THF to form sodium imidazolide. This reaction being exothermic, it was carried out at 0°C.

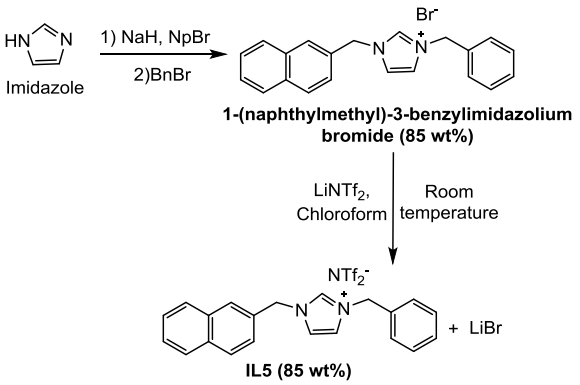

Scheme 1. Synthetic procedure for [(Np)(Bn)im][NTf_2] (**IL5**).

An equimolar amount of 2-(bromomethyl)naphthalene (17.96 g, 78 mmol) was dissolved in THF and added at room temperature. The mixture was stirred for 12 h. The obtained residue was washed with hexane (3×50 mL) to remove unreacted reagents (*i.e.*, imidazole and 2-(bromomethyl)naphthalene, namely NpBr) by filtration and 1-(naphthylmethyl)imidazole (15.51 g, 95 %) was obtained as a white powder. The quaternization of 1-(naphthylmethyl)imidazole was realized by addition of benzylbromide, namely BnBr (14.03 g, 82 mmol) to a solution of 1-

(naphthylmethyl)imidazole (15.51 g, 74 mmol) in 100 mL of acetonitrile (MeCN). After 12 h of stirring at room temperature, the resulting mixture was washed with hexane (3×50 mL) to remove excess of benzyl bromide. 1-(naphthylmethyl)-3-benzylimidazolium bromide (25.33 g, 66.6 mmol) was obtained as a beige solid after evaporation of MeCN under vacuum.
Finally, the anion exchange was realized by addition of a $LiNTf_2$ solution (19.31 g, 66.6 mmol in 20 mL of chloroform) to a solution of 1-(naphthylmethyl)-3-benzylimidazolium bromide (25.33 g, 66.6 mmol) in 50 mL of chloroform. The mixture was stirred at room temperature for 24 h and LiBr was filtered on sintered glass topped with celite. The obtained filtrate was washed with distilled water (3×50 mL) and the organic layer was concentrated using a rotary evaporator. After lyophilization, $[(Np)(Bn)im][NTf_2]$ (**IL5**) was obtained as a beige solid in 85 wt% yield. Melting point (Mp): 58.1 °C. The complete characterizations of $[(Np)(Bn)im][NTf_2]$ (**IL5**) can be found in the supplementary information section (Fig. S1, S2, S3).

^{1}H NMR: (500 MHz, $CDCl_3$) δ 9.08 (s, 1H), 8.13-6.88 (m, 14H), 5.50 (s, 2H), 5.34 (s, 2H). ^{13}C NMR: (126 MHz. $CDCl_3$) δ 135.74, 133.52, 133.20, 132.00, 129.85, 129.65, 129.31, 129.02, 128.93, 128.18, 127.82, 127.37, 127.12, 125.38, 122.18, 122.08, 119.88 (q, J = 2.56 Hz), 53.99, 53.82. Elemental analysis: % theoretical C: 47.667; H: 3.304; N: 7.250 and S: 11.065. Found C: 48.764, H: 3.467; N: 7.294 and S: 11.057.

2.3. Sonochemical exfoliation of natural graphite

In a typical procedure, a mass of 10 mg of natural graphite previously sieved to 50 µm (particle size < 50 µm) was introduced into a hemolysis tube to which 1 mL of IL was added. Note that the two solid ILs, namely $[(Bn)_2im][NTf_2]$ (**IL4**) and $[(Np)(Bn)im][NTf_2]$ (**IL5**), were heated to melt beforehand. Sonochemical exfoliation was carried out in an ultrasonic bath at a power input of 280 W and a frequency of 45 kHz for eight hours. The temperature was set at 60 °C in order to remain all dispersions in a liquid state. Centrifugation at 10,000 rpm was applied for one hour in order to recover the supernatant. The supernatant was named **G@ILn**, with n from 1 to 5 depending on the IL used (see Figure 1A). The determination of the concentration of carbonaceous material in the recovered supernatant was determined by mass difference between that of the graphite initially used and that of the graphite which precipitated after centrifugation. The latter was washed several times with chloroform to remove the residual ionic liquid and then dried in a vacuum oven at 80 °C.

*2.4. Preparation of the physical mixture made of natural graphite and $[(Np)(Bn)im]NTf_2$ (**IL5**)*

1 mL of melted 1-(naphthylmethyl)-3-benzylimidazolium bis(trifluoromethanesulfonyl)imide was introduced into a tube. After a few hours, the ionic liquid solidified; it was scraped and recovered to be gently mixed in a mortar with natural graphite (3.6 mg). The mass of natural graphite was set to closely match that of graphene in the analogous dispersion obtained by sonochemical exfoliation. The as-obtained mixture was named **G+IL5**. A similar procedure was applied to $[(Bn)_2im][NTf_2]$ (**IL4**), yielding **G+IL4**.

2.5. Characterization of the graphene dispersions

X-ray diffraction (XRD) was performed on solid ILs and graphene solid dispersions. The analyses were recorded on a Bruker D8 Advance diffractometer with a Bragg–Brentano geometry and equipped with a Bruker Lynx Eye detector, with the Kα radiation of Cu (λ = 1.5418 Å) and an angular step size of 0.02° into the 5°-50° interval. ^{1}H liquid-state NMR spectra were obtained using $SiMe_4$ as a reference on a Bruker 200. ^{1}H solid-state NMR was performed on a VNMR operator at 20 °C. Measurements of phase-transition temperatures were done with a differential scanning calorimeter, model DSC1 (METTLER TOLEDO). Samples of 10-15 mg were placed in an enclosure which temperature program was finely controlled through a conventional or inversely modulated thermal ramp and exposed to an argon flow atmosphere. Measurements for the melting and glass-transition temperatures were determined by cooling the sample to −150 °C, followed by heating from −150 to 200 °C at a rate of 5 °C/min. The glass transition was determined at the midpoint of a heat-capacity change, whereas the

melting temperatures were determined at the peak of the transition. Scanning electron microscopy (SEM) analyzes were performed on a Hitachi S-4800 electron microscope. Prior to observation, the dispersions were dissolved in chloroform and filtered directly on a PVDF membrane. Transmission electron microscopy (TEM) analyses were performed on a JEOL 1200 EXII microscope operating at 120 kV from MEA platform, Université de Montpellier. Raman spectroscopy was carried out on a Renishaw Labram spectrometer in microscopy mode and a 633 nm laser excitation.

3. Results and discussion

The sonochemical exfoliation of natural graphite was performed in an ultrasonic bath at 60 °C for 8 h. After centrifugation, homogeneous dispersions were recovered. For the IL without aromatic groups, *i.e.*, [Bmim][NTf_2] (**IL1**), the dispersion contained a very small amount of exfoliated carbon sheets (0.9 mg/mL; in good agreement with Wang *et al.* [15]) and were not stable (Fig. 1, Table S1). More concentrated dispersions were obtained with [(Bn)mim][NTf_2] (**IL2**) (2.4 mg/mL) and [(Np)mim][NTf_2] (**IL3**) (2.6 mg/mL).

Interestingly, these dispersions were stable (no sedimentation) for approximately four months, probably thanks to the aromatic side group, *i.e.*, benzyl and naphthylmethyl (Table S1). This result is in good agreement with previous works reported by Bari *et al.* [34] and Paduà *et al.* [36] with [(Bn)mim][NTf_2]. The last two ILs bearing two aromatic side groups, *i.e.*, [$(Bn)_2$im][NTf_2] (**IL4**) and [(Np)(Bn)im][NTf_2] (**IL5**), are solid at room temperature (Fig. 1). Their melting points, determined by DSC, are of 41.8 and 58.1 °C, respectively. Immediately after sonication, they gave liquid dispersions with high viscosity. For a few hours, they remained in a supercooled state, long enough to proceed with centrifugation before they began to gradually crystallize. Surprisingly, **IL4** was already reported in the literature for the exfoliation of graphite but without mentioning that it was a solid at room temperature [34]. One may assume that previously reported **IL4** contained impurities and/or traces of water that might significantly lower its melting point (see ^{1}H NMR of pure **IL4**, Fig. S6). The solidification/melting of the corresponding dispersions, namely **G@IL4** and **G@IL5**, was reversible without any alteration. Indeed, no precipitation were observed after several solidification/melting cycles, suggesting a remarkable long-term stability.

Moreover, the presence of two aromatic side groups on the imidazolium cation seems to favour dispersions with higher concentrations of exfoliated carbon sheets. Thus, a concentration of 4.6 mg/mL was obtained in **G@IL4** (in the same order of magnitude as shown by Bari *et al.* [34]), while a concentration of 3.6 mg/mL was obtained in **G@IL5**. These concentrations were significantly higher than those obtained with other ILs discussed above.

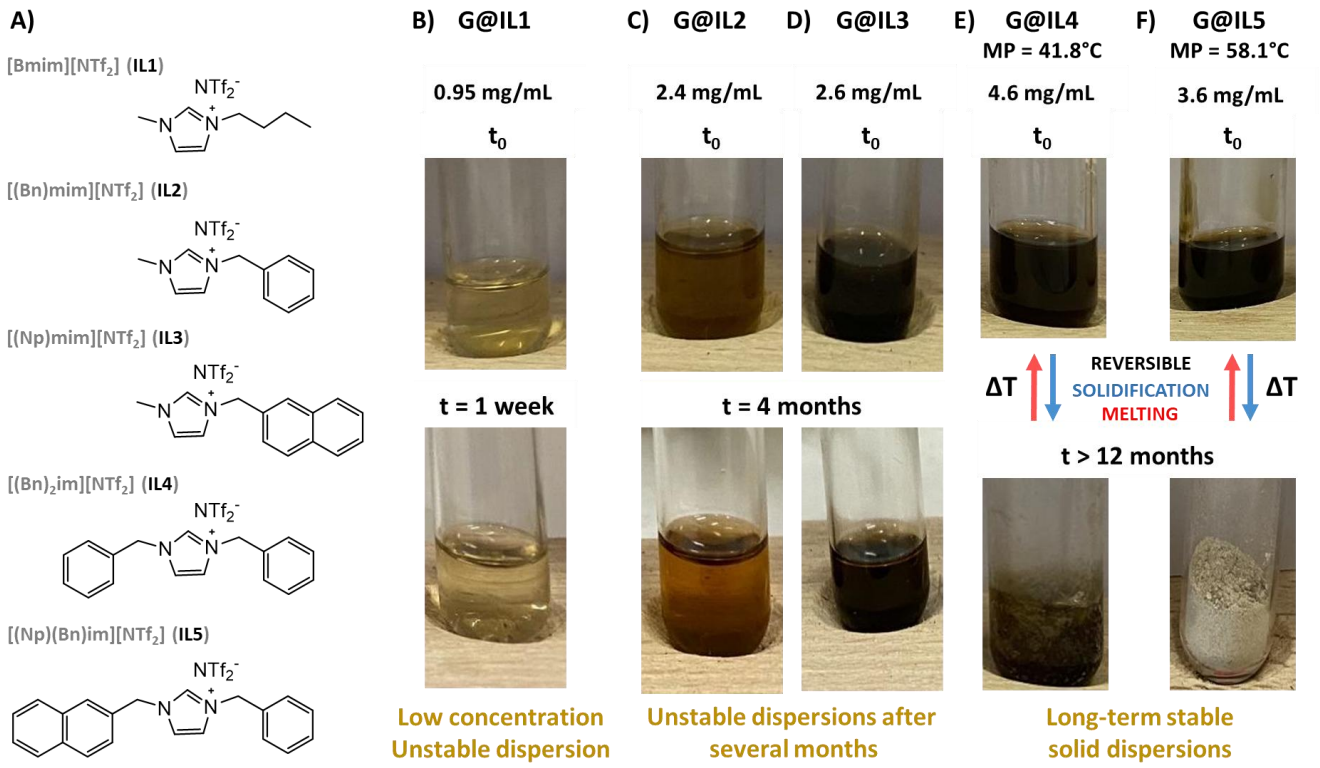

Fig. 1 (A) Ionic liquids used in our exfoliation process and dispersions recovered after sonication and centrifugation in (**B**) **IL1**: [Bmim][NTf_2] (unstable dispersion), (**C**) **IL2**: [(Bn)mim][NTf_2] (unstable dispersion after several months), (**D**) **IL3**: [(Np)mim][NTf_2] (unstable dispersion after several months), (**E**) **IL4**: [$(Bn)_2$im][NTf_2] (concentrated, long-term stable solid dispersion) and (**F**) **IL5**: [(Np)(Bn)im][NTf_2] (concentrated, long-term stable solid dispersion).

3.1. DSC analysis

Differential scanning calorimetry (DSC) was performed on the dispersions to get further insights into their thermal properties. **IL5** is mainly crystalline as shown by X-ray powder diffraction (XRD, Fig. 2A) and presents a well-defined melting peak in DSC (Fig. 2B), confirming its high crystallinity. The solid-to-liquid transition starts at 54.9 °C requiring a quantity of heat of 43.99 J/g and its meltdown completes at 58.1 °C. Besides, a glass transition is perceptible at −85.0 °C (Fig. 2B). The presence of carbon sheets in the dispersion caused significant differences both in the melting and in the glass transition peaks. The glass transition temperature (T_g) of the dispersion was lower than the one obtained for the pure IL (*i.e.*, −90 °C *versus* −85 °C; Fig. 2B). Glass transitions are characterized by very slow dynamics induced by the formation of cooperative rearrangement regions (CRR) with reduced local entropy [38-40]. In the case of **IL5**, that consists of ion pairs, *i.e.*, $[(Np)(Bn)im]^+$ cations in interaction with $[NTf_2]^-$ anions, the difference observed in the T_g can be attributed to a combination of several distinct phenomena: (i) an increase in the relative contribution of interface effects between **IL5** and exfoliated carbon sheets [41]; (ii) an overlap of the density distribution function of **IL5** and exfoliated carbon sheets leading to structural frustrations [42]; (iii) a change in CRR size [43] of **IL5**; and (iv) an induced gain in entropy [44] after exfoliation. In addition, slight decreases in both the melting onset temperature (T = 54.1 °C) and the melting point (MP = 57.6 °C) were noted for the dispersion (**G@IL5**). This feature validates the modification of the structure of the IL medium. One may also notice that in the presence of exfoliated carbon sheets, melting is slightly more endothermic with a melting enthalpy of 45.08 J/g (versus 43.99 J/g without exfoliated graphene sheets). This feature highlights the strong interaction between the imidazolium cation and the carbon sheets (Fig. 2B).

DSC experiments were also performed on the second solid dispersion obtained in [$(Bn)_2$im][NTf_2], namely **G@IL4**. As for **G@IL4**, the DSC did not show any variation in the T_g compared to the pure IL (T_g = −51.0 °C; see Fig. S7). However, the melting transition displayed two consecutive peaks that might be characteristic of a mixture of exfoliated graphite particles and IL without affecting the IL structure (Fig. S7). This can be attributed to the fact that the exfoliation did not lead to very thin graphene sheets capable of affecting the crystal lattice of **IL4**, in contrast to what has been observed with **IL5**. Nevertheless, **G@IL4** had a slightly higher melting temperature (MP = 43.6 °C) which required more energy (40.71 J/g) than for pure **IL4** (41.8 °C and 39.02 J/g, respectively). Moreover, **G@IL4** had a broader melting peak highlighting the strong interaction between the benzyl groups of the cation and the exfoliated carbon sheets (Fig. S7).

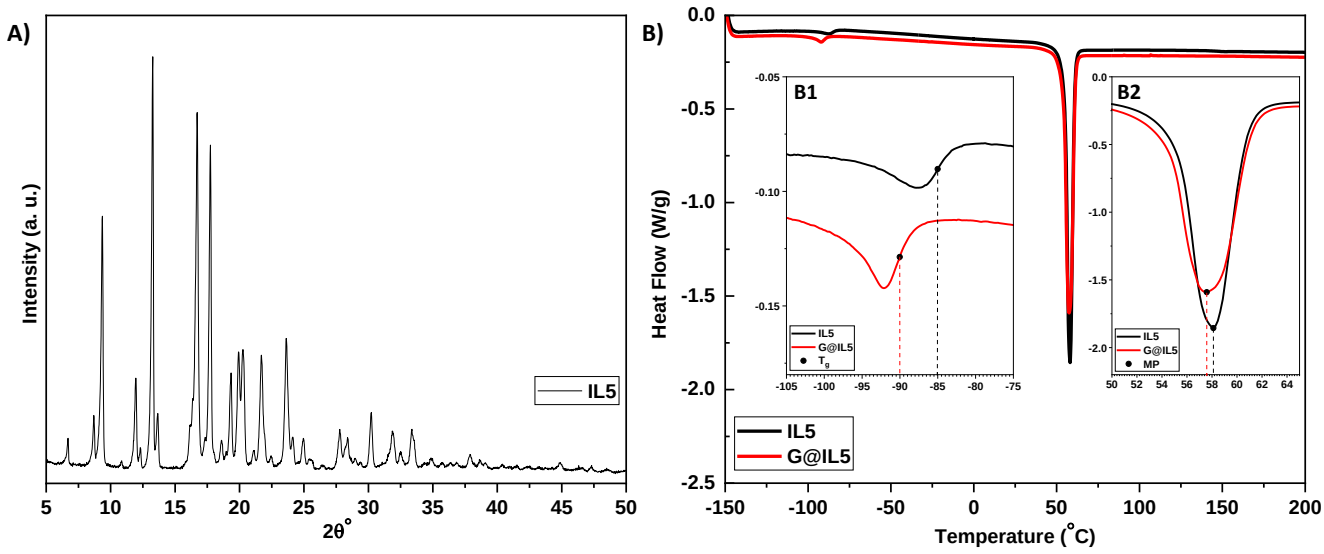

Fig. 2 (A) XRD pattern of pure **IL5** ([(Np)(Bn)im][NTf_2]) at room temperature, (B) DSC of **IL5** and **G@IL5** (*i.e.*, after graphite exfoliation) presenting two phenomena: (B1) glass transition and (B2) melting point.

DSC experiments were also performed on the liquid dispersions, namely **G@IL2** and **G@IL3**. **IL2** has a glass transition at a temperature of −57.1 °C with a thermal relaxation characteristic of the formation of denser regions during this transition due to the strong interactions between the cation $[(Bn)mim]^+$ and the anion $[NTf_2]^-$ [45]. The presence of the exfoliated carbon sheets in the dispersion (**G@IL2**) did not significantly affect the T_g (−57.4 °C) but caused the appearance of a small endothermic peak at −52.1 °C. This contribution might be characteristic of the presence of regions where the IL is in strong interaction with the carbon sheets (Fig. S8A). As for **IL3**, a 1.1 °C shift was observed for the T_g, from −37.0 °C for pure **IL3** to −35.9 °C for the dispersion **G@IL3** (Fig. S8B). This feature can be attributed to the strong interaction between the cation and the exfoliated carbon sheets favoring a closer packing and more ordered configuration of the aromatic imidazolium cation [46].

3.2. Solid-state static proton NMR

Solid-state static ^{1}H NMR was also performed on **G@IL4** and **G@IL5** at 20 °C, to maintain both dispersions in the solid-state. Interestingly, interactions between the $[(Np)(Bn)im]^+$ cation and the exfoliated carbon sheets were highlighted. The delocalized electrons of the carbon sheets generate their own magnetic field that acts on the protons of the imidazolium cation and more precisely on those of the aromatic groups. This feature causes a notable high field shift of 0.61 ppm from δ_{max} = 7.69 for pure **IL5** to δ_{max} = 7.08 for **G@IL5** (Fig. 3A) [47, 48]. Solid-state ^{1}H NMR under static conditions was also carried out on **IL4**. Broader peaks were obtained with **G@IL4** than with pure **IL4**. However, no clear shift was observed, suggesting that the interaction with the exfoliated carbon sheets are weaker than with **IL5** (Fig. S9). This feature is in good agreement with the DSC experiments.

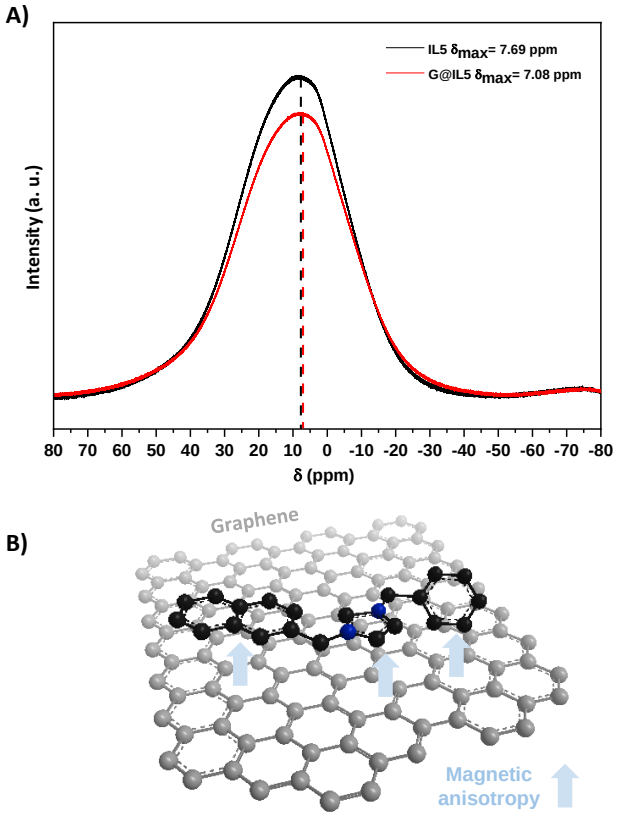

Fig. 3 A) Solid-state static ^{1}H NMR of **G@IL5**, B) schematic representation of the magnetic anisotropy of graphene on the ionic liquid **IL5**.

3.3. XRD analysis

To obtain further insights into the nature of the exfoliated carbon sheets in the solid dispersions, XRD measurements were carried out on **G@IL4** and **G@IL5**. Dispersions obtained after sonochemical exfoliation (**G@IL5**) were compared with physical mixtures of graphite and IL (**G+IL5**). Apart from the peaks related to the IL itself, the (002) Bragg

peak centered at *ca.* 26.5° *2θ* is characteristic of the distance between the stacked layers of carbon sheets in graphite [49].

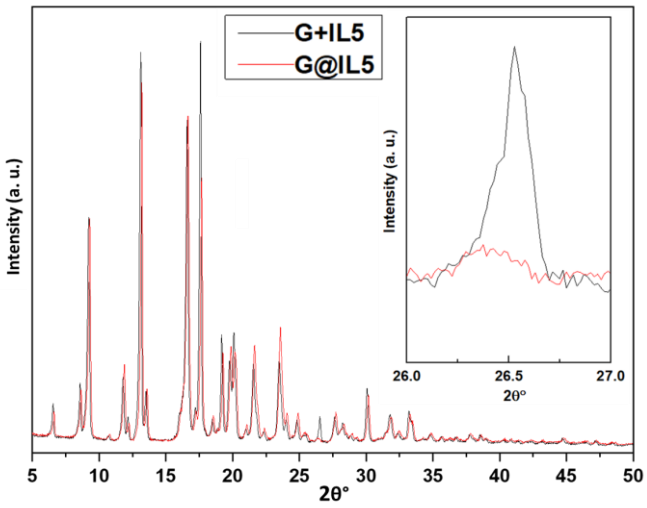

Fig. 4. XRD patterns of physical mixture of graphite-[(Np)(Bn)im][NTf_2] (**G+IL5**), and of their solid dispersion (**G@IL5**).

The shape and the position of this peak provide precious information about the nature of the exfoliated carbon sheets. In the physical mixture **G+IL5**, the (002) Bragg peak is still centered at 26.5° *2θ* (Fig. 4). This observation shows that graphite remained intact, although an asymmetrisation of the peak with a small shoulder at 26.4° *2θ* suggests some exfoliation *via* the intercalation of some ILs in graphite. Interestingly, in the dispersion obtained after sonochemical treatment, namely **G@IL5**, the (002) Bragg peak is much weaker and centered at 26.4° *2θ* (Fig. 4). This feature supports an efficient exfoliation of graphite and suggests the presence of isolated graphene sheets in the dispersion.
As for pure **IL4**, the XRD pattern shows peaks in the area of the (002) Bragg peak (Fig. S10). Thus, due to the strong overlap between **IL4** and graphite XRD patterns in **G@IL4**, we were not able to draw any conclusion on the effectiveness of the exfoliation in **IL4**.

3.4. Raman spectroscopy

To obtain further insights into the nature of the dispersed carbon sheets, Raman spectroscopy was also performed on the dispersions, using a laser excitation of 633 nm. It is important to point out that Raman spectroscopy experiments were made on the dispersions after more than 12 months of aging. Typically, graphite and graphene display three main bands: (i) the G band around 1580 cm^{-1} corresponding to C-C stretch modes of the sp^2 hybridized network; (ii) a dispersive D band in the range 1300-1350 cm^{-1} corresponding to second order double resonant modes activated by sp^3 defects; and (iii) the 2D band corresponding to second order double resonant modes, in the range 2600-2700 cm^{-1}. Ferrari *et al.* [50] reported that the width and the shape of the 2D band is characteristic for the number of graphene sheets in FLG deposited on a substrate [51]. Moreover, Bepete *et al.* reported the intrinsic Raman signatures of single-layer graphene dispersed in water [28]. Herein, it was impossible to characterize the dispersions both in the solid and in the liquid states because the aromatic ILs gave intense peaks in the same regions as those of the characteristic bands of graphene (Fig. S11). Thus, a dissolution of the dispersions in chloroform, followed by a vacuum filtration allowed the deposition of the dispersed carbon sheets on a PVDF membrane. In order to minimize the effects of the support on Raman spectroscopy, the membranes were partially dissolved in NMP before analysis.
The carbon material recovered from the physical mixture **G+IL5** displayed the same Raman signature as pristine natural graphite (G) (Fig. 5A and B). On the contrary, significant differences were observed in **G@IL5**. On the one hand, the G-band was centered at 1576 cm^{-1} with a 6 cm^{-1} downshift as compared with pristine graphite (G-band at 1582 cm^{-1}). Moreover, this band shows an asymmetrisation on the right flank which suggests the presence of a D' band. This feature supports the presence of defects, either punctual or related to a smaller lateral size of the layers after sonication. On the other hand, the 2D band displays a different shape, more symmetric, centered at 2660 cm^{-1} with a 26 cm^{-1} downshift as compared with the maximum observed with pristine graphite (2D-band at 2686 cm^{-1}) (Fig. 5C). These changes support the efficient exfoliation of graphite into FLG in **G@IL5** [51]. Note that the D-band at 1335 cm^{-1} and the D' band arise from defects already present in the starting graphite and additional defects caused by sonication. Unlike **G@IL5**, the Raman spectrum of **G@IL4** showed only slight differences as compared with pristine graphite, especially in the shape of the 2D band (Fig. S12). The G-band was centered at 1584 cm^{-1} (versus 1582 cm^{-1} for graphite), while the 2D-band was centered at the exact same position as the 2D-band of graphite. Nevertheless, the 2D-band in **G@IL4** does not show any graphite left shoulder. Besides, the D-band, centered at 1335 cm^{-1}, was more intense and larger than the one observed for pristine natural graphite (Fig. S12). These features suggest a slight modification of graphite during the sonochemical treatment in **G@IL4** without proving efficient exfoliation as in the case of **G@IL5**.

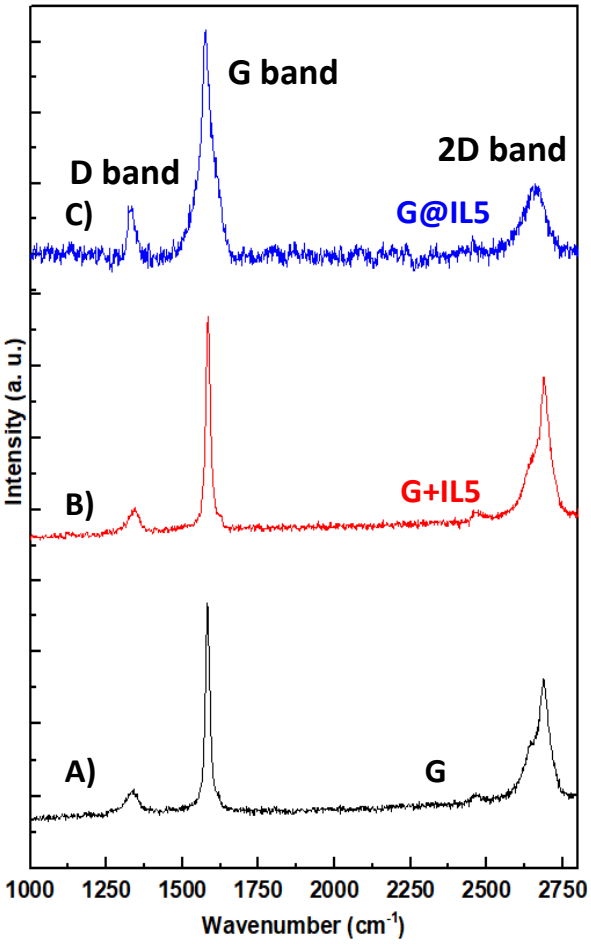

Fig. 5. Raman spectra of graphite G (A) and of carbon material recovered from IL-graphite physical mixture **G+IL5** (B) and of graphene recovered from the dispersion in [(Np)(Bn)im][NTf_2] **G@IL5** (C) (Normalization on G band).

Besides, Raman spectroscopy was performed on the carbon materials recovered from the liquid dispersions, following the same procedure as described above. Both **G@IL2** and **G@IL3** showed Raman spectra similar to the one obtained for pristine graphite. The Raman spectra displayed a narrow G band, a structured 2D band with a left shoulder and a weak D band compared to pristine graphite (Fig. S13, S14). These features suggest a selective dispersion of the largest sheets or those with the lowest amount of surface defects mainly due to strong π-π stacking between the aromatic groups of the imidazolium cations and the dispersed carbon sheets. However, it clearly indicates a less efficient exfoliation in **IL2** / **IL3** than in **IL4** and, to a larger extent, than in **IL5**. Overall, the exfoliation of graphite into graphene sheets is significantly more efficient in solid aromatic ILs, especially in **IL5**, in terms of stability, concentration and quality.

3.5. Scanning and transmission electron microscopy

To confirm the observations made by XRD and Raman spectroscopy, we studied the graphene dispersions after more than 12 months of aging. Before observation, the dispersions were dissolved in chloroform and filtrated on a PVDF membrane, following the same procedure as mentioned previously for Raman spectroscopy. It is worth noticing that the porous background that appears in the micrographs corresponds to the PVDF membrane (Fig. S15). Interestingly, thin and semi-transparent FLG sheets were perceptible for **G@IL5** (Fig. 6A), while bulky particles composed of stacked 2D carbon sheets were observed for pristine natural graphite (Fig. 6B, Fig. S16).

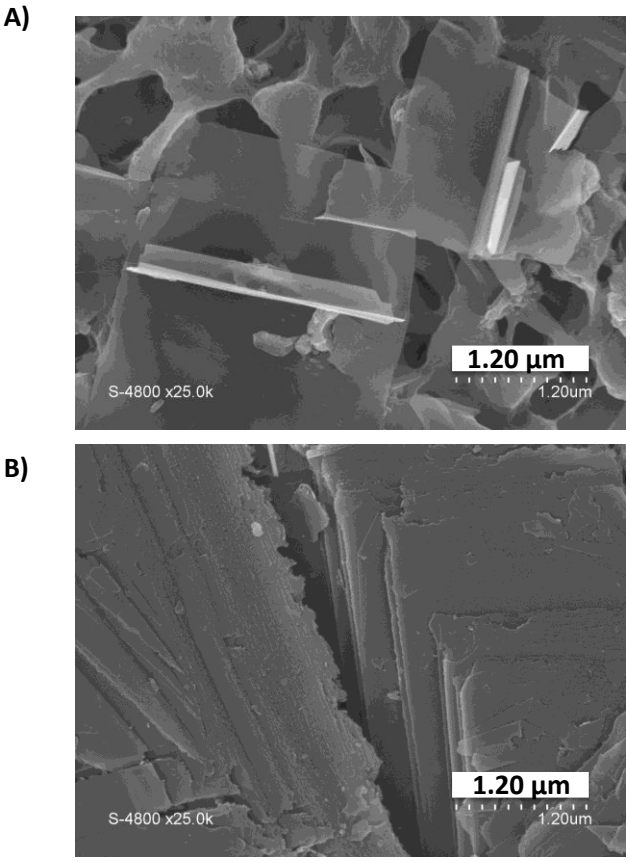

Fig.6. SEM images of (A) graphene sheets in **G@IL5** and (B) pristine natural graphite.

Unlike **G@IL5**, SEM micrographs of the carbon materials recovered from **G@IL4**, **G@IL3** and **G@IL2** showed thicker particles probably made of multiple stacked carbon sheets (Fig. S17-19). TEM was also performed after dissolution of a small amount of **G@IL5** in chloroform and drop casting on a Lacey carbon TEM grid. Thin, curved two-dimensional particles, made of a few layers of carbon sheets, were observed (Fig. 7). This observation supports the presence of FLG sheets in **G@IL5**, even after more than 12 months of aging, and confirms the efficient exfoliation of graphite in **IL5**.

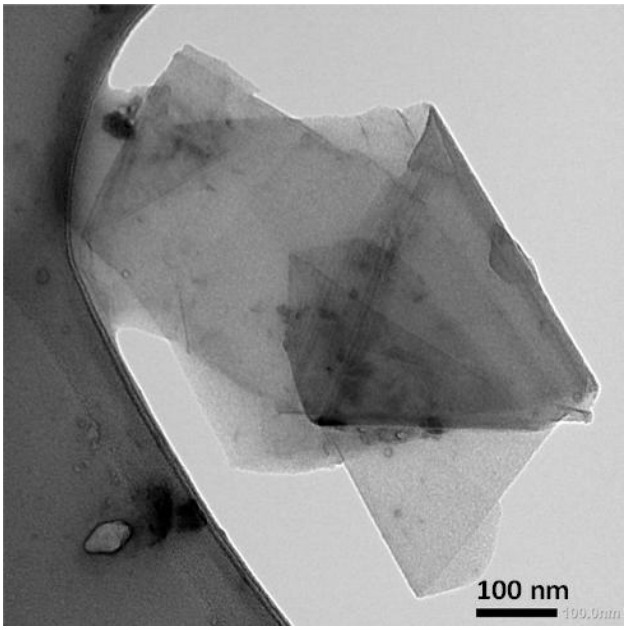

Fig.7. TEM image of graphene sheets in **G@IL5.**

4. Conclusion

To conclude, we described a newly engineered aromatic imidazolium-based IL, *i.e.*, 1-(naphthylmethyl)-3-benzylimidazolium bis(trifluoromethanesulfonyl)imide, [(Np)(Bn)im][NTf_2] (**IL5**), that is solid at room temperature. This highly aromatic IL was successfully used for the first time for the sonochemical exfoliation of graphite. We compared [(Np)(Bn)im][NTf_2] (**IL5**) with another imidazolium-based IL bearing a naphthylmethyl group, [(Np)mim][NTf_2] (**IL3**), and three imidazolium-based ILs that were already reported in the literature for the exfoliation of graphite [34] [35] [7]. We showed that the sonochemical exfoliation of graphite into graphene sheets was significantly more efficient in the two ILs bearing two aromatic side groups (*i.e.*, benzyl or naphthylmethyl) in terms of stability, concentration and quality. This feature was especially true in **IL5** and was supported by XRD, Raman spectroscopy and electron microscopy. Besides, strong interaction between the highly aromatic imidazolium cations of **IL5** and the graphene sheets were highlighted by solid-state NMR and DSC. In particular, significant differences were observed by DSC both in the melting and in the glass transition peaks of **IL5**, with a shift towards lower temperatures after exfoliation (**G@IL5**). This singular feature was not observed with **IL4** and demonstrates the modification of the structure of **IL5** due to the presence of exfoliated graphene sheets. In **IL5**, we obtained solid dispersions at room temperature (**G@IL5**) containing thin few layer graphene sheets with long-term stability (*ca.* up to 2 years) and high concentration (*ca.* 3.6 mg/mL). The high concentration reported herein is amongst the highest reported to date in the literature [7], far below the one reported by T. Aida *et al.* of *ca.* 23 mg/mL in imidazolium-based ILs with triethylene glycol bridges [52]. However, the value reported for **G@IL5** remains one or two orders of magnitude higher than the ones reported in water [28] or in organic solvents [29]. Interestingly, a long-term stability over more than 12 months, favored by the solid-state of the dispersion at room temperature, is unusual and opens the way to an easier processability of graphene dispersions. By a simple heating above 60 °C, the solid dispersion melts without any aggregation of the exfoliated layers (*i.e.*, no sedimentation). Such graphene dispersion offers both long-term stability in the solid-state and high processability in the liquid state, paving the way for the use of highly aromatic ILs to engineer concentrated graphene solid dispersions. Beyond graphene, we are currently studying analogous long-term stable dispersions using other nanocarbons for which we expect singular properties. Moreover, such long-term stable dispersion may be considered for the design and elaboration of functional materials for temperature-responsive ionic devices, such as membranes, sensors or electrochemical actuators [7].

Author Contributions

S.A. did the experimental work, synthesized the ionic liquids and wrote the first draft of the paper. N.B. and A.M. supervised and directed the work, conceived the project and wrote the paper. E.A. conducted Raman analyses and reviewed the paper. P.H. and I.B.M. supervised the work and reviewed the paper.

Corresponding Authors*
E-mail: nicolas.brun@enscm.fr
E-mail: ahmad.mehdi@umontpellier.fr
Ahmad Mehdi: 0000-0002-7830-2012
Nicolas Brun: 0000-0002-1013-311X

Acknowledgments

SA is grateful to Lebanese University for financial support. Several characterizations were performed with the support of the "Balard Plateforme d'Analyses et de Caractérisation" (PAC Balard). The authors would like to thank Amine Geneste and Pr. Jean Pierre Habas for the DSC experiments and the fruitful discussions, Emmanuel Fernandez for the solid-state ^{1}H NMR experiments, Bernard Fraisse for the XRD analyses and Didier Cot (IEM) for the SEM observations. The authors would like to acknowledge Franck Godiard from the MEA platform, Université de Montpellier, for the TEM experiments.

References

1. Patel, D.D. and J.M. Lee, *Applications of ionic liquids.* The Chemical Record, 2012. **12**(3): p. 329-355.
2. Wasserscheid, P. and T. Welton, *Ionic liquids in synthesis*. Vol. 1. 2008: Wiley Online Library.
3. Ho, T.D., et al., *Ionic liquids in analytical chemistry: fundamentals, advances, and perspectives.* Analytical Chemistry, 2014. **86**(1): p. 262-285.
4. Docherty, K.M. and C.F. Kulpa Jr, *Toxicity and antimicrobial activity of imidazolium and pyridinium ionic liquids.* Green Chemistry, 2005. **7**(4): p. 185-189.
5. Erythropel, H.C., et al., *The Green ChemisTREE: 20 years after taking root with the 12 principles.* Green chemistry, 2018. **20**(9): p. 1929-1961.
6. Chiappe, C. and D. Pieraccini, *Ionic liquids: solvent properties and organic reactivity*. Journal of Physical Organic Chemistry, 2005. **18**(4): p. 275-297.
7. Aldroubi, S., et al., *When graphene meets ionic liquids: a good match for the design of functional materials.* Nanoscale, 2021. **13**(5): p. 2750-2779.
8. Ravula, S., et al., *Ionic liquid-assisted exfoliation and dispersion: stripping graphene and its two-dimensional layered inorganic counterparts of their inhibitions.* Nanoscale, 2015. **7**(10): p. 4338-4353.
9. Chaban, V.V. and E.E. Fileti, *Graphene exfoliation in ionic liquids: unified methodology.* RSC advances, 2015. **5**(99): p. 81229-81234.
10. Chaban, V.V., E.E. Fileti, and O.V. Prezhdo, *Exfoliation of graphene in ionic liquids: pyridinium versus pyrrolidinium.* The Journal of Physical Chemistry C, 2017. **121**(1): p. 911-917.
11. Bordes, É., J. Szala-Bilnik, and A.A. Pádua, *Exfoliation of graphene and fluorographene in molecular and ionic liquids.* Faraday discussions, 2018. **206**: p. 61-75.
12. Gupta, H. and J. Texter, *Ionic-liquid-based polyurethane dispersions for stabilizing graphene in water.* MRS Advances, 2019. **4**(41-42): p. 2289-2298.
13. Biswas, R., *Molecular dynamics studies on the exfoliation of graphene in room temperature ionic liquids.* Journal of Molecular Liquids, 2021. **337**: p. 116592.
14. Jamaluddin, N.A., et al., *Fabrication and application of composite adsorbents made by one-pot electrochemical exfoliation of graphite in surfactant ionic liquid/nanocellulose mixtures.* Physical Chemistry Chemical Physics, 2021. **23**(35): p. 19313-19328.
15. Wang, X., et al., *Direct exfoliation of natural graphite into micrometre size few layers graphene sheets using ionic liquids.* Chemical Communications, 2010. **46**(25): p. 4487-4489.
16. Hernandez, Y., et al., *High-yield production of graphene by liquid-phase exfoliation of graphite.* Nature nanotechnology, 2008. **3**(9): p. 563-568.
17. Elbourne, A., et al., *Molecular resolution in situ imaging of spontaneous graphene exfoliation.* The Journal of Physical Chemistry Letters, 2016. **7**(16): p. 3118-3122.
18. Reddy, A.S. and G.N. Sastry, *Cation [M= H+, Li+, Na+, K+, Ca2+, Mg2+, NH4+, and NMe4+] interactions with the aromatic motifs of naturally occurring amino acids: a theoretical study.* The Journal of Physical Chemistry A, 2005. **109**(39): p. 8893-8903.
19. Björk, J., et al., *Adsorption of aromatic and anti-aromatic systems on graphene through π− π stacking.* The Journal of Physical Chemistry Letters, 2010. **1**(23): p. 3407-3412.
20. Parviz, D., et al., *Dispersions of non-covalently functionalized graphene with minimal stabilizer.* Acs Nano, 2012. **6**(10): p. 8857-8867.
21. Zu, S.-Z., D. Zhou, and B.-H. Han, *Supramolecular surface modification and*

dispersion of graphene in water and organic solvents. Journal of Nanoscience and Nanotechnology, 2013. **13**(2): p. 946-953.
22. Yang, Y., D. Shi, and T. Jiang, *Non‐covalent Exfoliation of Graphite to Produce Graphene.* Non‐covalent Interactions in the Synthesis and Design of New Compounds, 2016: p. 413-429.
23. Xu, Y., et al., *Liquid-phase exfoliation of graphene: an overview on exfoliation media, techniques, and challenges.* Nanomaterials, 2018. **8**(11): p. 942.
24. Htwe, Y., et al., *Effect of electrolytes and sonication times on the formation of graphene using an electrochemical exfoliation process.* Applied Surface Science, 2019. **469**: p. 951-961.
25. Cravotto, G. and P. Cintas, *Sonication‐assisted fabrication and post‐synthetic modifications of graphene‐like materials.* Chemistry–A European Journal, 2010. **16**(18): p. 5246-5259.
26. Notley, S.M., *Highly concentrated aqueous suspensions of graphene through ultrasonic exfoliation with continuous surfactant addition.* Langmuir, 2012. **28**(40): p. 14110-14113.
27. Khan, U., et al., *High‐concentration solvent exfoliation of graphene.* small, 2010. **6**(7): p. 864-871.
28. Bepete, G., et al., *Surfactant-free single-layer graphene in water.* Nature Chemistry, 2017. **9**(4): p. 347-352.
29. Salavagione, H.J., et al., *Identification of high performance solvents for the sustainable processing of graphene.* Green Chemistry, 2017. **19**(11): p. 2550-2560.
30. Pénicaud, A. and C. Drummond, *Deconstructing graphite: graphenide solutions.* Accounts of chemical research, 2013. **46**(1): p. 129-137.
31. Milner, E.M., et al., *Structure and morphology of charged graphene platelets in solution by small-angle neutron scattering.* Journal of the American Chemical Society, 2012. **134**(20): p. 8302-8305.
32. Catheline, A., et al., *Solutions of fully exfoliated individual graphene flakes in low boiling point solvents.* Soft Matter, 2012. **8**(30): p. 7882-7887.
33. Tran, T.S., N.K. Dutta, and N.R. Choudhury, *Poly (ionic liquid)-stabilized graphene nanoinks for scalable 3D printing of graphene aerogels.* ACS Applied Nano Materials, 2020. **3**(11): p. 11608-11619.
34. Bari, R., et al., *Direct exfoliation of graphene in ionic liquids with aromatic groups.* Colloids and Surfaces A: Physicochemical and Engineering Aspects, 2014. **463**: p. 63-69.
35. Godoy, A.P., et al., *Ultrasound exfoliation of graphite in biphasic liquid systems containing ionic liquids: a study on the conditions for obtaining large few-layers graphene.* Ultrasonics Sonochemistry, 2019. **55**: p. 279-288.
36. Bordes, E., et al., *Dispersion and stabilization of exfoliated graphene in ionic liquids.* Frontiers in chemistry, 2019. **7**: p. 223.
37. Xu, J., et al., *Liquid-phase exfoliation of graphene in organic solvents with addition of naphthalene.* Journal of colloid and interface science, 2014. **418**: p. 37-42.
38. Tracht, U., et al., *Length scale of dynamic heterogeneities at the glass transition determined by multidimensional nuclear magnetic resonance.* Physical Review Letters, 1998. **81**(13): p. 2727.
39. Mézard, M. and G. Parisi, *Thermodynamics of glasses: A first principles computation.* Journal of Physics: Condensed Matter, 1999. **11**(10A): p. A157.
40. Stevenson, J.D., J. Schmalian, and P.G. Wolynes, *The shapes of cooperatively rearranging regions in glass-forming liquids.* Nature Physics, 2006. **2**(4): p. 268-274.
41. Alcoutlabi, M. and G.B. McKenna, *Effects of confinement on material behaviour at the nanometre size scale.* Journal of Physics: Condensed Matter, 2005. **17**(15): p. R461.
42. McCoy, J.D. and J.G. Curro, *Conjectures on the glass transition of polymers in confined geometries.* The Journal of chemical physics, 2002. **116**(21): p. 9154-9157.
43. Anastasiadis, S., et al., *Nanoscopic-confinement effects on local dynamics.*

Physical Review Letters, 2000. **84**(5): p. 915.
44. Gupta, P.K. and J.C. Mauro, *The configurational entropy of glass.* Journal of non-crystalline solids, 2009. **355**(10-12): p. 595-599.
45. Dzyuba, S.V. and R.A. Bartsch, *Influence of structural variations in 1- alkyl (aralkyl)- 3- methylimidazolium hexafluorophosphates and bis (trifluoromethylsulfonyl) imides on physical properties of the ionic liquids.* ChemPhysChem, 2002. **3**(2): p. 161-166.
46. Zuo, Y., et al., *The effect of nanoconfinement on the glass transition temperature of ionic liquids.* Physical Chemistry Chemical Physics, 2019. **21**(1): p. 22-25.
47. Forse, A.C., et al., *Ring current effects: factors affecting the NMR chemical shift of molecules adsorbed on porous carbons.* The Journal of Physical Chemistry C, 2014. **118**(14): p. 7508-7514.
48. Bichenkova, E.V., et al., *NMR detects molecular interactions of graphene with aromatic and aliphatic hydrocarbons in water.* 2D Materials, 2017. **5**(1): p. 015003.
49. Johra, F.T., J.-W. Lee, and W.-G. Jung, *Facile and safe graphene preparation on solution based platform.* Journal of Industrial and Engineering Chemistry, 2014. **20**(5): p. 2883-2887.
50. Ferrari, A.C., et al., *Raman spectrum of graphene and graphene layers.* Physical review letters, 2006. **97**(18): p. 187401.
51. Das, S., et al., *Localized in situ polymerization on graphene surfaces for stabilized graphene dispersions.* ACS applied materials & interfaces, 2011. **3**(6): p. 1844-1851.
52. Matsumoto, M., et al., *Ultrahigh-throughput exfoliation of graphite into pristine 'single-layer'graphene using microwaves and molecularly engineered ionic liquids.* Nature chemistry, 2015. **7**(9): p. 730-736.